Check for updates

Zhaoxia Rao
School of Engineering,
Brown University,
Providence, RI 02912
e-mail: zhaoxia_rao@brown.edu

Hanxun Jin
School of Engineering,
Brown University,
Providence, RI 02912
e-mail: hanxun_jin@brown.edu

Alison Engwall
School of Engineering,
Brown University,
Providence, RI 02912
e-mail: alison_engwall@alumni.brown.edu

Eric Chason
School of Engineering,
Brown University,
Providence, RI 02912
e-mail: eric_chason@brown.edu

Kyung-Suk Kim[1]
School of Engineering,
Brown University,
Providence, RI 02912
e-mail: kyung-suk_kim@brown.edu

Determination of Stresses in Incrementally Deposited Films From Wafer-Curvature Measurements

We report closed-form formulas to calculate the incremental-deposition stress, the elastic relaxation stress, and the residual stress in a finite-thickness film from a wafer-curvature measurement. The calculation shows how the incremental deposition of a new stressed layer to the film affects the amount of the film/wafer curvature and the stress state of the previously deposited layers. The formulas allow the incremental-deposition stress and the elastic relaxation to be correctly calculated from the slope of the measured curvature versus thickness for arbitrary thicknesses and biaxial moduli of the film and the substrate. Subtraction of the cumulative elastic relaxation from the incremental-deposition stress history results in the residual stress left in the film after the whole deposition process. The validities of the formulas are confirmed by curvature measurements of electrodeposited Ni films on substrates with different thicknesses. [DOI: 10.1115/1.4047572]

Keywords: stress analysis, thin films, wafer curvature, elasticity, micromechanics, structures

Downloaded from http://asmedigitalcollection.asme.org/appliedmechanics/article-pdf/87/10/101006/6548607/jam_87_10_101006.pdf by guest on 25 April 2024

1 Introduction

Residual stress in thin films is a persistent and challenging problem for many applications, motivating many studies of it [1–3]. Wafer-curvature measurement during thin-film deposition is a popular technique for determining the evolution of residual stress in a film [4]. A schematic of an apparatus for such measurements (multi-beam optical stress sensor (MOSS) [5]) is shown in Fig. 1(*a*). It is a common practice that the stress in the layer caused by incremental deposition is determined by measuring the change in the curvature with film thickness [6,7]. However, the evaluation of the stress in incrementally deposited films has been based on a severely limited thin-film approximation on the elastic deformation of the film/substrate system. Here, we derive a general stress-evaluation formula for the growth of incrementally deposited finite-thickness films and experimentally verify the accuracy of the formula.

When a solid film is grown on a substrate by incremental deposition of atoms, the incremental process of solid-film formation on the surface of the growing film creates stress in the newly deposited layer. From a mechanics point of view, the stress formation in the incremental layer is regarded as if a thin elastic incremental layer is pre-stretched and glued on the surface of the growing film, followed by the release of the pre-stretching end forces. Here, the incremental-deposition stress stands for the self-equilibrium stress in the incremental layer after the release of the pre-stretching end forces. In the rest of the paper, we abbreviate the incremental-deposition stress as "ID stress." The ID stress induces the increment of wafer curvature, and the incremental change of curvature with thickness is proportional to the ID stress unless microstructural relaxation processes such as subsurface grain growth are occurring. The curvature variation, then, elastically and cumulatively relaxes the stress in the previously grown part of the film, in response to successive incremental-deposition processes.

In previous treatments of wafer-curvature analysis, there were two critical flaws in evaluating the residual stress distribution in an incrementally deposited film of finite thickness [1–4]. One is that stress relaxation in the underlying layers has been ignored or assumed negligible when new layers are deposited. The other is the thin-film approximation in which the effects of the thickness and the modulus of the film are ignored, underestimating the bending stiffness of the growing film/substrate composite structure. The cumulative underestimation of the bending stiffness requires a significant correction factor to obtain the ID stress from curvature measurements. Besides, the overall distribution of the stress relaxation made during the film growth has to be subtracted from the ID stress distribution to obtain the resultant residual stress in the film. In this paper, we derive closed-form formulas for the correction factor of the ID stress and the cumulative relaxation stress to get the resultant residual stress.

A schematic of the film growth and the stress distribution in the film are shown on an undeformed configuration in Fig. 1(*b*), where $\sigma(y; h_f)$ represents the stress at a distance y from the interface for a film thickness h_f. Since a film is often grown over an interfacial binding layer on the substrate, the effects of a binding layer of thickness h_b are included in the analysis in Appendix. Throughout the paper, we denote normalized variables with a "hat," for which the substrate thickness h_s normalizes position or length variables, and the substrate biaxial modulus M_s normalizes stress variables; $\hat{\sigma}(\hat{y}; \hat{h}_f) = \sigma(y/h_s; h_f/h_s)/M_s$, $\hat{h}_b = h_b/h_s$, and $\hat{M}_f = M_f/M_s$. Here, M represents the biaxial modulus, $M = E/(1-\nu)$, of Young's modulus E and Poisson's ratio ν. The subscripts f, s, and b imply film, substrate, and binding layer respectively. The deformation is assumed to be within the limit of linear-elasticity analysis [8], and h_s much smaller than the lateral dimension of the substrate, so that edge effects near the periphery of the substrate are negligible. In Ref. [8], the validity limit of linear-elasticity analysis is provided,

[1]Corresponding author.

Contributed by the Applied Mechanics Division of ASME for publication in the JOURNAL OF APPLIED MECHANICS. Manuscript received April 10, 2020; final manuscript received May 21, 2020; published online July 8, 2020. Assoc. Editor: Yong Zhu.

 Copyright © 2020 by ASME

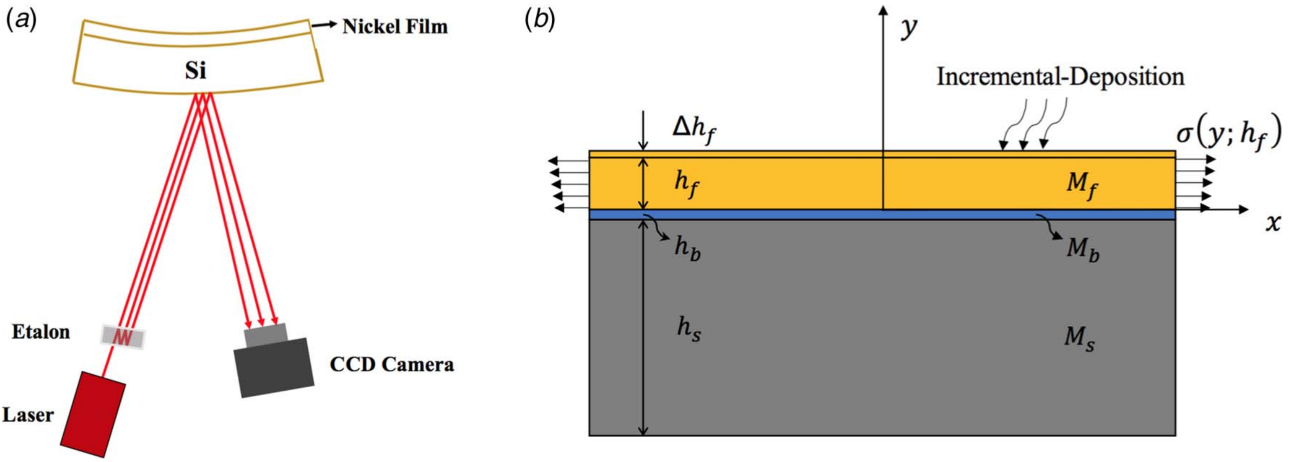

Fig. 1 (*a*) Schematic of MOSS for real-time curvature measurement used for Ni films electrodeposited onto a Si substrate and (*b*) schematic of the deposition of an incremental film layer Δh_f to the previously deposited film with thickness h_f. The binding layer with thickness h_b is deposited to the substrate with thickness h_s.

based on the large-deflection analysis of a thin bimaterial plate with a misfit strain, but not for general incremental deposition.

2 Growth of a Finite-Thickness Film on a Homogeneous Substrate

For a configuration of incremental solid-film deposition on a substrate, we begin with a simple case with no binding layer, $h_b = 0$. At this point, we consider the substrate homogeneous and linear elastic, and the stress distribution on the cross section, $-h_s \le y \le h_f$, is in self-equilibrium so that the net force and moment on the cross section vanish

$$\int_{-h_s}^{h_f} \sigma(y;\, h_f)\, dy = 0 \tag{1a}$$

$$\int_{-h_s}^{h_f} y\sigma(y;\, h_f)\, dy = 0 \tag{1b}$$

Here, $\sigma(y;\, h_f)$ refers to the residual stress at y in a film with thickness h_f, for $0 < y \le h_f$. Then, the residual stress $\sigma(h_f;h_f)$ at $y = h_f$ is the ID stress $\sigma_{\rm ID}(h_f)$ of the film with thickness h_f. However, note that, in general, the ID stress $\sigma_{\rm ID}(y)(=\sigma(y;\, y))$ is not the same as the residual stress $\sigma(y;\, h_f)$ at $y \ne h_f$ in the film with thickness h_f. Once the stress distribution in the substrate is expressed in terms of the interface curvature $\kappa_{(i)}$ and the interface-stretch strain $\epsilon_{(i)}$ as

$$\sigma(y;\, h_f) = M_s(-\kappa_{(i)} y + \epsilon_{(i)}) \quad \text{for} \quad -h_s \le y \le 0 \tag{2}$$

insertion of Eq. (2) into Eqs. (1*a*) and (1*b*), followed by nondimensionalization, yields

$$\hat{\kappa}_{(i)} = 6\int_0^{\hat{h}_f} \hat{\sigma}(\hat{y};\, \hat{h}_f) d\hat{y} + 12\int_0^{\hat{h}_f} \hat{y}\hat{\sigma}(\hat{y};\, \hat{h}_f) d\hat{y} \tag{3a}$$

for which $\hat{\kappa}_{(i)} = h_s \kappa_{(i)}$, and

$$\epsilon_{(i)} = -4\int_0^{\hat{h}_f} \hat{\sigma}(\hat{y};\, \hat{h}_f) d\hat{y} - 6\int_0^{\hat{h}_f} \hat{y}\hat{\sigma}(\hat{y};\, \hat{h}_f)\, d\hat{y} \tag{3b}$$

The second term on the right-hand side of Eq. (3*a*) is the second-order term of $\hat{h}_f$, i.e., $O(\hat{h}_f^2)$, and is usually neglected for a very thin film, $\hat{h}_f \ll 1$. The first term of Eq. (3*a*) stands for the traditional Stoney formula [9] of wafer curvature caused by thin-film deposition.

By taking derivatives of Eqs. (3*a*) and (3*b*) with respect to $\hat{h}_f$, we obtain

$$\frac{d\hat{\kappa}_{(i)}}{d\hat{h}_f} = 6\hat{\sigma}(\hat{h}_f;\, \hat{h}_f) + 6\int_0^{\hat{h}_f} \frac{\partial \hat{\sigma}(\hat{y};\, \hat{h}_f)}{\partial \hat{h}_f} d\hat{y} + 12\hat{h}_f \hat{\sigma}(\hat{h}_f;\, \hat{h}_f) + 12\int_0^{\hat{h}_f} \hat{y}\frac{\partial \hat{\sigma}(\hat{y};\, \hat{h}_f)}{\partial \hat{h}_f} d\hat{y} \tag{4a}$$

and

$$\frac{d\epsilon_{(i)}}{d\hat{h}_f} = -4\hat{\sigma}(\hat{h}_f;\, \hat{h}_f) - 4\int_0^{\hat{h}_f} \frac{\partial \hat{\sigma}(\hat{y};\, \hat{h}_f)}{\partial \hat{h}_f} d\hat{y} - 6\hat{h}_f \hat{\sigma}(\hat{h}_f;\, \hat{h}_f) - 6\int_0^{\hat{h}_f} \hat{y}\frac{\partial \hat{\sigma}(\hat{y};\, \hat{h}_f)}{\partial \hat{h}_f} d\hat{y} \tag{4b}$$

where $\hat{\sigma}(\hat{h}_f;\, \hat{h}_f)$ is the ID stress and the term $\partial\hat{\sigma}(\hat{y};\, \hat{h}_f)/\partial\hat{h}_f$ represents the rate of stress relaxation on the cross section of the film, caused by the deposition-induced elastic and inelastic deformation of the film.

Next, we consider the resultant residual stress distribution in the growing film as the sum of the ID stress, $\hat{\sigma}(\hat{y};\, \hat{y})$, and the relaxation stress, $\hat{\sigma}_{rel}(\hat{y};\, \hat{h}_f)$

$$\hat{\sigma}(\hat{y};\, \hat{h}_f) = \hat{\sigma}(\hat{y};\, \hat{y}) + \hat{\sigma}_{rel}(\hat{y};\, \hat{h}_f) \tag{5a}$$

Unless inelastic deformation is taking place due to subsurface microstructural rearrangement of materials in the film, the relaxation stress, $\hat{\sigma}_{rel}(\hat{y};\, \hat{h}_f)$, is solely instigated by the elastic bending-stretching relaxation, $\hat{\sigma}_e(\hat{y};\, \hat{h}_f)$, as

$$\hat{\sigma}_{rel}(\hat{y};\, \hat{h}_f) = \hat{\sigma}_e(\hat{y};\, \hat{h}_f) = \hat{M}_f[-\{\hat{\kappa}_{(i)}(\hat{h}_f) - \hat{\kappa}_{(i)}(\hat{y})\}\hat{y} + \{\varepsilon_{(i)}(\hat{h}_f) - \varepsilon_{(i)}(\hat{y})\}] \tag{5b}$$

Downloaded from http://asmedigitalcollection.asme.org/appliedmechanics/article-pdf/87/10/101006/6548607/jam_87_10_101006.pdf by guest on 25 April 2024

Thereafter, taking derivatives of Eqs. (5*a*) and (5*b*) with respect to $\hat{h}_f$ leads to

$$\frac{\partial \hat{\sigma}(\hat{y}; \hat{h}_f)}{\partial \hat{h}_f} = \frac{\partial \hat{\sigma}_e(\hat{y}; \hat{h}_f)}{\partial \hat{h}_f} = \hat{M}_f \left[-\hat{y} \frac{d\hat{\kappa}_{(i)}(\hat{h}_f)}{d\hat{h}_f} + \frac{d\varepsilon_{(i)}(\hat{h}_f)}{d\hat{h}_f} \right] \tag{6}$$

Then, insertion of Eq. (6) into Eqs. (4*a*) and (4*b*) gives the ID stress for the growth of a finite-thickness film in terms of the curvature variation rate as

$$\hat{\sigma}_{\rm ID}(\hat{h}_f) = \hat{\sigma}(\hat{h}_f; \hat{h}_f) = \frac{1}{6} \left\{ 1 + \hat{M}_f \hat{h}_f \left(\frac{4 - 2/\hat{M}_f + 5\hat{h}_f + 4\hat{h}_f^2 + \hat{M}_f \hat{h}_f^3}{1 + 2\hat{h}_f + \hat{M}_f \hat{h}_f^2} \right) \right\} \frac{d\hat{\kappa}_{(i)}}{d\hat{h}_f} \tag{7}$$

For a thin film, $\hat{h}_f \ll 1$, Eq. (7) brings down to the first-order formula with respect to $\hat{h}_f$ as

$$\hat{\sigma}_{\rm ID}^{(1)}(\hat{h}_f) = \frac{1}{6} \left\{ 1 + \hat{M}_f \hat{h}_f \left(4 - \frac{2}{\hat{M}_f} \right) \right\} \frac{d\hat{\kappa}_{(i)}}{d\hat{h}_f} \tag{7a}$$

Equation (7*a*) can be further reduced to the zeroth-order formula of the traditional thin-film approximation

$$\hat{\sigma}_{\rm ID}^{(0)}(\hat{h}_f) = \frac{1}{6} \frac{d\hat{\kappa}_{(i)}}{d\hat{h}_f} \tag{7b}$$

Equation (7*b*) has been traditionally derived from the Stoney formula [9] and widely used to evaluate the final residual stress in the film with wafer-curvature measurements for the growth of thin films [10,11] as $\hat{\sigma}(\hat{y}; \hat{h}_f) \approx \hat{\sigma}_{\rm ID}^{(0)}(\hat{y})$, ignoring the stress-relaxation term $\hat{\sigma}_{rel}(\hat{y}; \hat{h}_f)$ in Eq. (5*a*). However, the relaxation term is not negligible for growth of finite-thickness films. Furthermore, the conventional evaluation with the zeroth-order term, $\hat{\sigma}_{\rm ID}^{(0)}(\hat{h}_f)$, substantially underestimates the true ID stress $\hat{\sigma}_{\rm ID}(\hat{h}_f)$ expressed in Eq. (7), for film growth on a relatively thin substrate. In Sec. 3, we show the significance of the correction factor of the ID stress evaluation, the curly bracket term in Eq. (7), as well as of the stress relaxation term, Eq. (5*b*), in real experiments.

3 Experiment

The experimental studies were based on previous measurements of stress in a Ni film electrodeposited over a Cu layer on a silicon wafer [12]. Although the grain size changed with film thickness, it did not change after the growth was stopped. Multiple studies showed that the stress evolution was very reproducible for multiple runs during deposition under identical conditions. Therefore, we could expect that the ID stress distribution would be the same for films grown on different substrate thicknesses if the same growth conditions were used.

The samples were initially prepared by evaporating 10 nm Ti followed by 150 nm Cu onto (100) Si substrates. The Ti layer was deposited to improve the adhesion with the substrate, and the Cu layer was deposited for conduction. Ni films were subsequently electrodeposited at room temperature under galvanostatic control using a saturated calomel electrode (SCE) reference. The Ni was continuously deposited to a maximum thickness of 19.4 μm at a growth rate of 3.30 nm/s with an electrolyte concentration of 0.36 mol/l nickel sulfamate and 0.65 mol/l boric acid.

Curvature measurements were done using the MOSS technique [5]. This method monitors the changes in spacing between parallel laser beams which are reflected from the side of the substrate that is not deposited on during the deposition. The curvature resolution of the MOSS system is 1.6×10^{-4} m^{-1}, providing a sensitivity of 0.1 N/m for a Si wafer substrate with a thickness of 155 μm. The growth was made on substrates with thicknesses of 460 μm and 155 μm. The lateral dimension of both samples is 33 mm × 10 mm. The sample was clamped at one end, but finite element method (FEM) calculations confirm that the curvature deviates from an unclamped sample by less than 1%.

X-ray diffraction measurements showed that the Ni samples had a strong <111> fiber texture, i.e., the grains in the film have their <111> axis normal to the surface, while the orientation in the plane of the film is random. In this case, the biaxial modulus for the Ni is calculated to be 389.3 GPa [13]. The substrate is single crystal Si with a (100) orientation, so its biaxial modulus is 180.3 GPa [14].

4 Results and Discussion

Curvature measurements for the films grown on the two different substrate thicknesses (155 μm and 460 μm) are presented in Fig. 2(*a*). The curvature measured on the thin substrate is seen to be much larger than that from the thick substrate because of the dependence of the curvature on $1/h_s^2$ in the leading order of Eq. (3*a*). In Fig. 2(*b*), this curvature data are normalized by $M_s h_s^2/6$ to obtain the Stoney estimate of the stress-thickness. Surprisingly, the Stoney stress-thickness curves are distinctively different between the two. Because the films were prepared in the same way, the ID stress distribution should be the same in both. Therefore, we attribute the difference to the effect of the different substrate thicknesses, not well contemplated in the conversion factor, $M_s h_s^2/6$, derived from the Stoney formula of thin-film approximation. In the following discussion, for detailed comparison, we perform stress calculations using the values of the substrate thicknesses and the biaxial moduli from the experimental studies. Equation (A3) reveals that error made by neglecting the copper interlayer is less than 0.2% for the thin substrate and less than 0.03% for the thick substrate. Therefore, Eq. (7) is used to evaluate the ID stress for the following discussion, neglecting the effect of the copper interlayer.

The correction factor over $M_s h_s^2/6$ of Eq. (7*b*), $F(\hat{h}_f)$ which is the term in the curly bracket of Eq. (7), is shown as a function of the film thickness for the two different substrates in Fig. 2(*c*). When the film is thin, the ratio is close to 1, as $F(0) = 1$, so that the ID stress approaches the value obtained from the Stoney equation. As long as the substrate is much thicker than the surface or the interface stress layer of the substrate, the Stoney limit of Eq. (7), $F(0) = 1$, is valid. The Stoney formula's validity can break down for an early stage inhomogeneous coverage of atomic deposition on the substrate surface, but the limit thickness in which the validity of using the Stoney formula breaks down is very small and could not be determined with the experimental resolution in Figs. 2(*a*) and 2(*b*).

Beyond the limit thickness, the correction increases with the film thickness, which means that the slope of the stress-thickness is lower for the same value of the ID stress as the film gets thicker. This can be understood by thinking of the effect of the previously deposited layers on the bending stiffness of the underlying film/substrate combination as the film thickness increases. The thicker the underlying structure becomes, the less curvature is induced for additional layers of the stressed film. The correction is larger for the thinner substrate since it increasingly depends on the ratio of film thickness to substrate thickness. For the thinner substrate, the ID stress differs by 5% from the amount estimated by the Stoney when the thickness is only 1.1 μm. The same 5% deviation occurs for the thicker substrate when the film is 3.4 μm. For the maximum film thickness (19.4 μm) on the 155-μm substrate, the ID stress determined from the slope of the stress-thickness is almost a factor of 2 different from the value that would be incorrectly obtained without the thickness correction.

Downloaded from http://asmedigitalcollection.asme.org/appliedmechanics/article-pdf/87/10/101006/6548607/jam_87_10_101006.pdf by guest on 25 April 2024

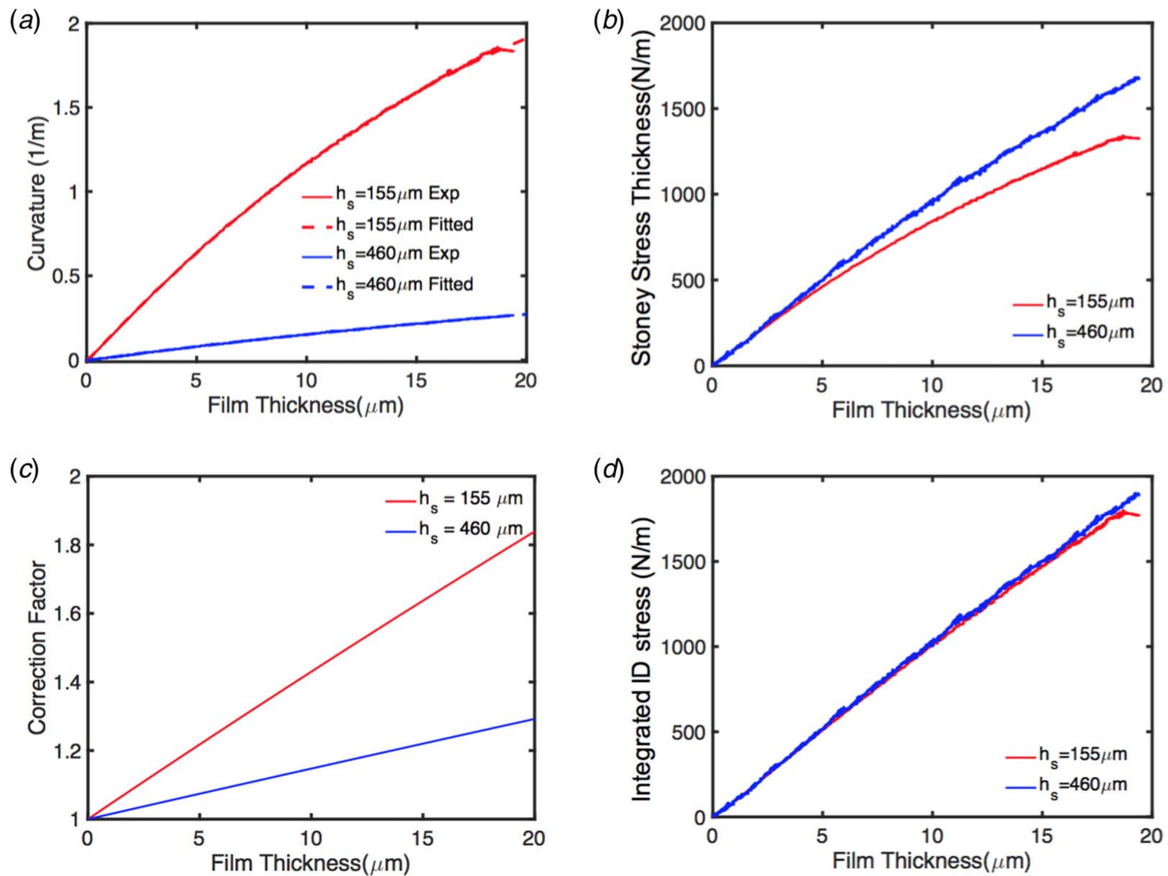

Fig. 2 (*a*) Measured curvature evolution of Ni films deposited onto two different Si substrates with thicknesses, 155 μm and 460 μm. The dashed lines represent the curves fitted by cubic equations. (*b*) Estimated stress-thickness by normalizing the curvature data with $M_s h_s^2/6$ for Stoney's calculation. (*c*) Correction factor for two different substrate thicknesses h_s, 155 μm and 460 μm. (*d*) Integrated ID stress versus thickness for two different substrate thicknesses h_s,155 μm and 460 μm.

For the measured curvature, we cannot assume a priori that the ID stress is constant with thickness. In this case, the correct stress-thickness is obtained by inserting the curvature versus film thickness data of Fig. 2(*a*) into the integrated form of Eq. (7);

$$\begin{aligned}\int_0^{\hat{h}_f} \hat{\sigma}_{\mathrm{ID}}(\hat{y})d\hat{y} &= \frac{1}{6}\int_0^{\hat{h}_f} F(\hat{y})\frac{d\hat{\kappa}_{(i)}}{d\hat{y}}d\hat{y} \\ &= \frac{1}{6}F(\hat{h}_f)\hat{\kappa}_{(i)}(\hat{h}_f) - \frac{1}{6}\int_0^{\hat{h}_f}\hat{\kappa}_{(i)}(\hat{y})\frac{dF}{d\hat{y}}d\hat{y}\end{aligned} \tag{8}$$

The integrated ID stress for the two substrate thicknesses after this correction is shown in Fig. 2(*d*).

In contrast to the Stoney stress-thickness curves shown in Fig. 2(*b*), the two sets of the integrated ID stress data shown in Fig. 2(*d*) are very similar, consistent with our expectation that the ID stress is the same in both sets of deposition.

Next, to understand how the residual stresses are distributed in the two different films, at first, the ID stresses in the films are calculated and plotted in Figs. 3(*a*) and 3(*b*). We evaluate the ID stresses in the films with Eq. (7) in which the curvature rates, $d\hat{\kappa}/d\hat{h}_f$, are calculated by differentiating the cubic-polynomial best-fits of the

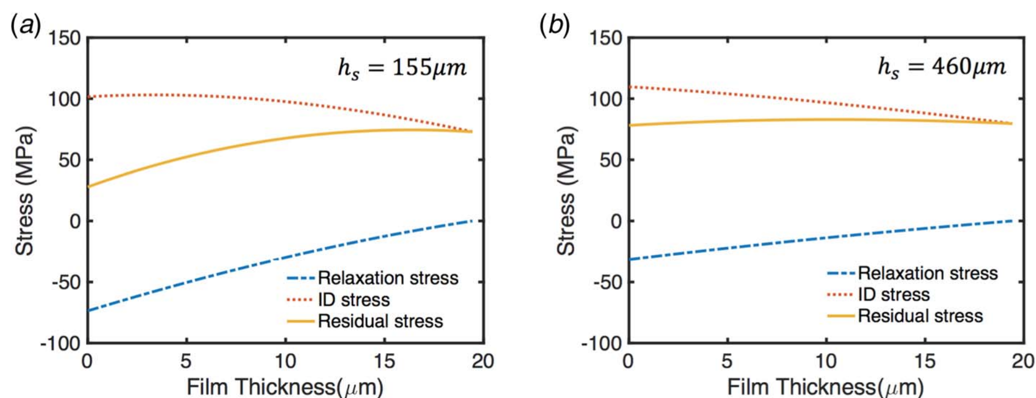

Fig. 3 The ID stress, relaxation stress, and residual stress distribution for (*a*) $h_s = 155$ μm and (*b*) $h_s = 460$ μm

Downloaded from http://asmedigitalcollection.asme.org/appliedmechanics/article-pdf/87/10/101006/6548607/jam_87_10_101006.pdf by guest on 25 April 2024

experimental curvature versus film thickness data in Fig. 2(*a*). The two ID stresses exhibited in Figs. 3(*a*) and 3(*b*) are indeed very close, decreasing with film thickness. The observed decrease of the ID stress with thickness [15] is consistent with a measured increase in the grain size at the surface, which decreases the tensile contribution from the coalescence of grains [6]. When a stress-loaded film is grown, the grain size coarsens [15], or the surface roughness grows [16], effectively reducing the deposition stress as the film grows thicker.

The ID stresses are, then, subtracted by relaxation stresses, Eq. (5*b*), to get the residual stress distributions in the films, also shown in Figs. 3(*a*) and 3(*b*). The stress relaxations in the films grown on the substrates of two different thicknesses are very different, and in turn, the resultant residual stresses are distinctive as well. The residual stress in the film deposited on the 155 μm-thick substrate has a noticeable gradient across the film thickness, while that on the 460 μm-thick substrate is almost constant. The greater degree of relaxation stress as the thickness increases has implications for applications such as Ni microelectromechanical system (MEMS) [17]. Even if the ID stress is constant with thickness, our results predict that the residual stress will have a larger gradient in the film grown on a thinner substrate. A large stress gradient can lead to significant curvature in the film when it is removed from the substrate and hence deformation in the desired device [17]. It is also noted here that if the film is grown under intense ion beam bombardment in a sputtering deposition, the effects of subsurface microstructural rearrangement [18] have to be taken into account in evaluating the residual stress in Eq. (5*b*).

5 Summary

In conclusion, we have derived closed-form formulas to calculate the ID stress, the elastic relaxation, and the residual stress in an incrementally deposited film of finite thickness, from wafer-curvature measurements. The thin-film approximation employed in the conventional Stoney formula was relaxed in the derivation. In the derivation, we considered the curvature change induced by adding a stressed incremental layer to the film under the assumption that the stress in the previously deposited layer is only relaxed by elastic bending and stretching due to the curvature change in subsequent deposition processes. Calculations and experimental measurements show that the same stressed layer induces a smaller change in the curvature as the film grows thicker, and the variation and its consequence on the residual stress become significant as the relative film thickness to the substrate thickness gets larger. The formulas have been experimentally validated and made the accuracy of the residual stress measurement substantially improved to precisely assess stress-driven microstructural evolution in film growth by incremental deposition.

Acknowledgment

We gratefully acknowledge supports for this work from the NSF awards DMR-1602491 and CMMI-1934314.

Conflict of Interest

There are no conflicts of interest.

Data Availability Statement

The datasets generated and supporting the findings of this article are obtainable from the corresponding author upon reasonable request. The authors attest that all data for this study are included in the paper.

Appendix: Growth of a Finite-Thickness Film on a Bilayer Substrate

The wafer-curvature experiment is often used to measure the stress in the film deposited over a binding-layer, which is predeposited between the film and the substrate. A configuration of the double-layer deposition is depicted in Fig. 1(*b*). The self-equilibrium equations of force and moment balance over the entire cross section are, respectively, derived as for Eqs. (2*a*) and (2*b*):

$$\frac{\hat{\kappa}_{(i)}(1+2\hat{h}_b+\hat{M}_b\hat{h}_b^2)}{2(1+\hat{M}_b\hat{h}_b)}+\epsilon_{(i)}+\frac{1}{(1+\hat{M}_b\hat{h}_b)}\int_0^{\hat{h}_f}\hat{\sigma}(\hat{y};\,\hat{h}_f)d\hat{y}=0 \tag{A1a}$$

and

$$-\frac{2\hat{\kappa}_{(i)}(1+3\hat{h}_b+3\hat{h}_b^2+\hat{M}_b\hat{h}_b^3)}{3(1+2\hat{h}_b+\hat{M}_b\hat{h}_b^2)}-\epsilon_{(i)}+\frac{2}{(1+2\hat{h}_b+\hat{M}_b\hat{h}_b^2)}\int_0^{\hat{h}_f}\hat{y}\hat{\sigma}(\hat{y};\,\hat{h}_f)\,d\hat{y}=0 \tag{A1b}$$

Thereafter, the curvature of the interface between the film and the binding layer is obtained as

$$\hat{\kappa}_{(i)}=6C_1\int_0^{\hat{h}_f}\hat{\sigma}(\hat{y};\,\hat{h}_f)d\hat{y}+12C_2\int_0^{\hat{h}_f}\hat{y}\hat{\sigma}(\hat{y};\,\hat{h}_f)d\hat{y} \tag{A2}$$

where the binding layer constants are $C_1=(1+2\hat{h}_b+\hat{M}_b\hat{h}_b^2)/D$ and $C_2=(1+\hat{M}_b\hat{h}_b)/D$ for which $D=1+4\hat{M}_b\hat{h}_b+6\hat{M}_b\hat{h}_b^2+4\hat{M}_b\hat{h}_b^3+M_b^2\hat{h}_b^4$.

Following the same procedure as for finite-thickness film deposition on a homogeneous substrate from Eqs. (3*a*)–(7), we get the ID stress for the growth of a finite-thickness film on a bilayer substrate as

$$\hat{\sigma}_{\rm ID}^{(b)}(\hat{h}_f)=\frac{D_1}{6D_2}\frac{d\hat{\kappa}_{(i)}}{d\hat{h}_f} \tag{A3}$$

where

$$\begin{aligned}D_1&=(1+\hat{M}_b\hat{h}_b)+\hat{M}_f\{1+3C_1(1+2\hat{h}_b+\hat{M}_b\hat{h}_b^2)\}\hat{h}_f\\&\quad+3\hat{M}_f\{C_1(1+\hat{M}_b\hat{h}_b)+C_2(1+2\hat{h}_b+\hat{M}_b\hat{h}_b^2)\}\hat{h}_f^2\\&\quad+4C_2\hat{M}_f(1+\hat{M}_b\hat{h}_b)\hat{h}_f^3+C_2\hat{M}_f^2\hat{h}_f^4\end{aligned} \tag{A3a}$$

and

$$D_2=C_1(1+\hat{M}_b\hat{h}_b)+2C_2\hat{h}_f(1+\hat{M}_b\hat{h}_b)+C_2\hat{M}_f\hat{h}_f^2 \tag{A3b}$$

When the binding layer thickness vanishes, $\hat{h}_b\to 0$, both constants C_1 and C_2 become unity, and Eq. (A3) merges to the formula Eq. (7) for finite-thickness film deposition on a homogeneous substrate. Order analysis of Eqs. (A3*a*) and (A3*b*) reveals that if $\hat{M}_b\hat{h}_b\ll 1$, we can safely use Eq. (7) to evaluate the film stress. Here, it is noted that stress distribution in the binding layer and the substrate is the superposition of the stress caused by the binding layer deposition and that by the subsequent film deposition.

References

[1] Doerner, M. F., and Nix, W. D., 1988, "Stresses and Deformation Processes in Thin Films on Substrates," Crit. Rev. Solid State Mater. Sci., **14**(3), pp. 225–268.
[2] Koch, R., 1994, "The Intrinsic Stress of Polycrystalline and Epitaxial Thin Metal Films," J Phys.: Condens. Matter, **6**(45), pp. 9519–9550.
[3] Abadias, G., Chason, E., Keckes, J., Sebastiani, M., Thompson, G. B., Barthel, E., Doll, G. L., Murray, C. E., Stoessel, C. H., and Martinu, L., 2018, "Review Article: Stress in Thin Films and Coatings: Current Status, Challenges, and Prospects," J. Vac. Sci. Technol. A, **36**(2), p. 020801.
[4] Freund, L. B., and Suresh, S., 2003, *Thin Film Materials: Stress, Defect Formation and Surface Evolution*, Cambridge University Press, Cambridge.
[5] Floro, J. A., Chason, E., and Lee, S. R., 1995, "Real Time Measurement of Epilayer Strain Using a Simplified Wafer Curvature Technique," MRS Proc., **405**, p. 381.

Downloaded from http://asmedigitalcollection.asme.org/appliedmechanics/article-pdf/87/10/101006/6548607/jam_87_10_101006.pdf by guest on 25 April 2024

[6] Chason, E., 2012, "A Kinetic Analysis of Residual Stress Evolution in Polycrystalline Thin Films," Thin Solid Films, **526**, pp. 1–14.
[7] Chason, E., and Guduru, P. R., 2016, "Tutorial: Understanding Residual Stress in Polycrystalline Thin Films Through Real-Time Measurements and Physical Models," J. Appl. Phys., **119**(19), p. 191101.
[8] Freund, L. B., Floro, J. A., and Chason, E., 1999, "Extensions of the Stoney Formula for Substrate Curvature to Configurations With Thin Substrates or Large Deformations," Appl. Phys. Lett., **74**(14), pp. 1987–1989.
[9] Stoney, G. G., 1909, "The Tension of Metallic Films Deposited by Electrolysis," Proc. R. Soc. Lond. A, **82**(553), pp. 172–175.
[10] Chason, E., and Engwall, A. M., 2015, "Relating Residual Stress to Thin Film Growth Processes via a Kinetic Model and Real-Time Experiments," Thin Solid Films, **596**, pp. 2–7.
[11] Chason, E., Shin, J. W., Hearne, S. J., and Freund, L. B., 2012, "Kinetic Model for Dependence of Thin Film Stress on Growth Rate, Temperature, and Microstructure," J. Appl. Phys., **111**(8), p. 083520.
[12] Rao, Z., Hearne, S. J., and Chason, E., 2019, "The Effects of Plating Current, Grain Size, and Electrolyte on Stress Evolution in Electrodeposited Ni," J. Electrochem. Soc., **166**(1), pp. D3212–D3218.
[13] Hurth, J. P., and Loath, J., 1983, *Theory of Dislocations*, 2nd ed., Krieger Publishing Company, FL.
[14] Janssen, G. C. A. M., Abdalla, M. M., Van Keulen, F., Pujada, B. R., and Van Venrooy, B., 2009, "Celebrating the 100th Anniversary of the Stoney Equation for Film Stress: Developments From Polycrystalline Steel Strips to Single Crystal Silicon Wafers," Thin Solid Films, **517**(6), pp. 1858–1867.
[15] Engwall, A. M., Rao, Z., and Chason, E., 2016, "Origins of Residual Stress in Thin Films: Interaction Between Microstructure and Growth Kinetics," Mater. Des., **110**(13), pp. 616–623.
[16] Kim, K.-S., Hurtado, J. A., and Tan, H., 1999, "Evolution of a Surface-Roughness Spectrum Caused by Stress in Nanometer-Scale Chemical Etching," Phys. Rev. Lett., **83**(19), pp. 3872–3875.
[17] Matovic, J., 2006, "Application of Ni Electroplating Techniques Towards Stress-Free Microelectromechanical System-Based Sensors and Actuators," Proc. Inst. Mech. Eng., Part C: J. Mech. Eng. Sci., **220**(11), pp. 1645–1654.
[18] Kim, S.-P., Chew, H. B., Chason, E., Shenoy, V. B., and Kim, K.-S., 2012, "Nanoscale Mechanisms of Surface Stress and Morphology Evolution in FCC Metals Under Noble-Gas Ion Bombardments," Proc. R. Soc. A: Math. Phys. Eng. Sci., **468**(2145), pp. 2550–2573.

Downloaded from http://asmedigitalcollection.asme.org/appliedmechanics/article-pdf/87/10/101006/6548607/jam_87_10_101006.pdf by guest on 25 April 2024